Early Paleozoic ridge subduction in the Chinese Altai: Insight from the abrupt change in zircon Hf isotopic compositions

SUN Min[1†], LONG XiaoPing[1,2], CAI KeDa[1], JIANG YingDe[1], WANG BuYun[1], YUAN Chao[2], ZHAO GuoChun[1], XIAO WenJiao[3] & WU FuYuan[3]

[1] Department of Earth Sciences, The University of Hong Kong, Pokfulam Road, Hong Kong, China;

[2] Key Laboratory of Isotope Geochronology and Geochemistry, Guangzhou Institute of Geochemistry, Chinese Academy of Sciences, Guangzhou 510640, China;

[3] State Key Laboratory of Lithospheric Evolution, Institute of Geology and Geophysics, Chinese Academy of Sciences, Beijing 100029, China

Zircons were separated from granitoids, gneisses, and sedimentary rocks of the Chinese Altai. Those with igneous characteristics yielded U-Pb ages of 280－2800 Ma, recording a long history of magmatic activity in the region. Zircon Hf isotopic compositions show an abrupt change at ~420 Ma, indicating that prior to that time the magmas came from both ancient and juvenile sources, whereas younger magmas were derived mainly from juvenile material. This may imply that the lithosphere was significantly modified in composition by a rapid addition of melt from the mantle. We suggest that this dramatic change was due to the onset of ridge subduction, which can account not only for the formation of voluminous granitoids, mafic rocks with complex compositions, and the association of adakite + high-Mg andesite+boninite + Nb-enriched basalt, but also for the coeval high-*T,* low-*P* metamorphism.

Paleozoic, ridge subduction, Hf isotope, granite, Altai

Zircon is ideal for Hf isotopic study, because the crystal chemistry of zircon allows entrain of large amounts of Hf, but not Lu, thus the radiogenic daughter of ^{176}Hf from the decay of ^{176}Lu is extremely low in zircon, and the ^{176}Hf/^{177}Hf ratios of the zircon reflect those of the precursor magma[1]. Significant advances have been made on zircon Hf isotopic systematics, for example the Laboratory of Lithospheric Evolution in the Institute of Geology and Geophysics, Chinese Academy of Sciences has contributed greatly to the technological aspects of this work.

For this study, samples were collected from granitoids, gneisses, and sedimentary rocks of different age in the Chinese Altai and analyzed in the above-mentioned Laboratory of Lithospheric Evolution. Our results show an abrupt change in zircon Hf isotopic compositions at ~420 Ma, which may be result of an important regional geological event. Based on an evaluation of the regional geology, geochemical data, and metamorphic development, we suggest that the observed change may mark the onset of ridge subduction. We plan to test this model with further research.

1 Geological background

The Altai orogenic belt, a part of the Central Asian Orogenic Belt[2], transects the northern part of Xinjiang in China and extends westward to Kazakhstan and Russia and eastward to Mongolia. It lies south of the Sayan

Block of Siberia and is separated from the Kazakhstan-Junggar Block farther south by the Erqis Fault[3]. The belt is characterized by voluminous granitoids and volcanic rock-bearing accretionary complexes, many of which host world-class ore deposits[4−15]. Therefore, a detailed study of the geological evolution of the region is important for understanding the orogenic process of the Central Asian Orogenic Belt, determining the origin of the mineral deposits, and guiding future mineral exploration.

Based on the stratigraphy, rock associations, style of deformation, and type of metamorphism and deformation, previous workers divided the region into six NW-SE-trending, fault-bounded terranes[2,3,16] (Figure 1). The Habahe Group, the oldest sedimentary sequence in the region, is composed mainly of sandstone, siltstone, mudstone, and slate. It has been variously assigned to the middle-upper Ordovician[17], Sinian[18,19], or Sinian-Cambrian[20]. A U-Pb isotopic study on detrital zircon from these sedimentary rocks yielded ages mainly between 460−540 Ma, with metamorphic overgrowth rims having an age of ~384 Ma, indicating deposition of

the rocks between mid-Ordovician and Early Devonian[21]. Geochemical data indicate that the original sediments were immature and derived locally from intermediate-silicic arc magmatic rocks[22]. Hence, the Chinese Altai was an active continental margin in the Early Paleozoic[21−24], contrary to previous interpretations[25].

The high-grade gneiss provides another key element for understanding the evolutionary history of the region. The widely distributed paragneiss was originally considered to be the metamorphic equivalent of the Habahe Group, but was later assigned to Paleo-Meso-proterozoic Kemuqun Group and the Neoproterozoic Fuyun Group[26,27]. Thus, some workers interpreted these rocks to be part of the Precambrian basement[2,3] and a microcontinent model was also proposed[25]. However, our previous U-Pb geochronological study showed that the nearly all of the zircons from these rocks have ages of 466−528 Ma[24]. Because these ages were obtained from zircon cores with good oscillatory zoning and high Th/U ratios and the ages are similar to those of the Habahe Group, we consider that these gneisses are the
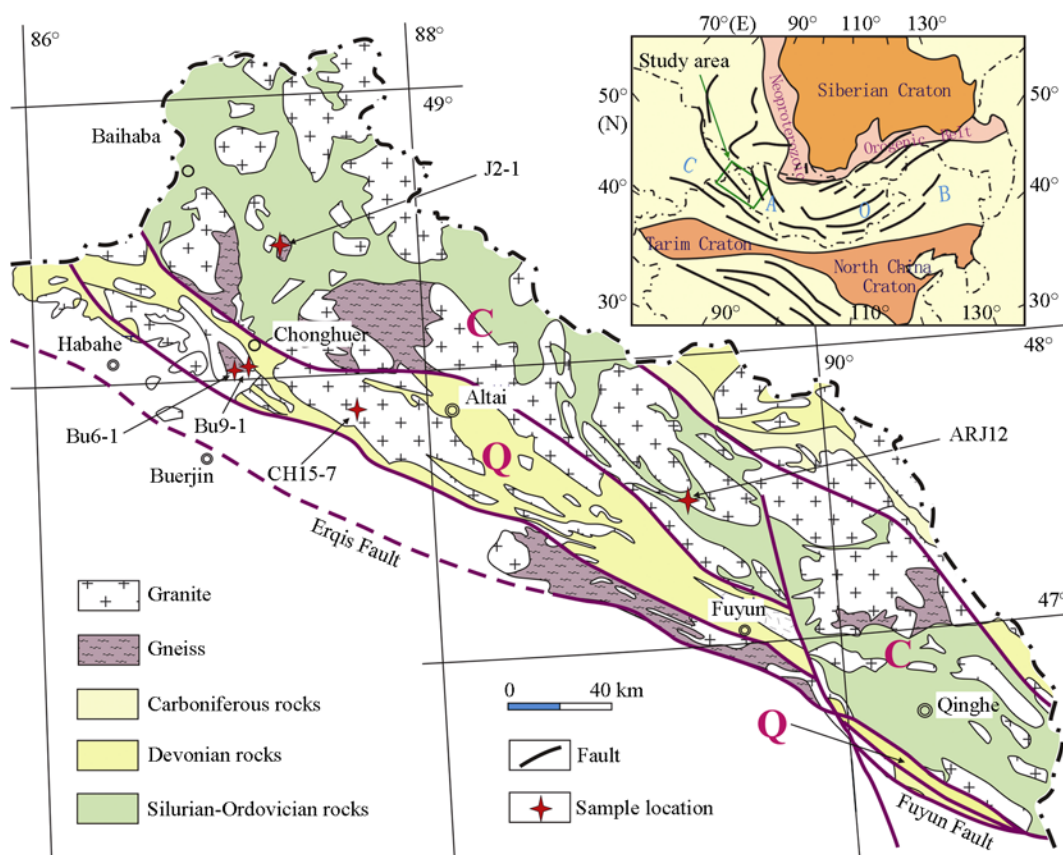
Figure 1 Geological map of the Chinese Altai (modified from He et al.[2] and Windley et al.[3]). Domains: C, Central Altai; Q, Qiongkuer.

metamorphic equivalent of the Habahe rocks[24]. Thus, our data do not support the micro-continent model.

Granitoids also crop out widely in the Chinese Altai, where exposures make up more than 40% of the region[2,28,29]. The granitoids, which are mainly biotite granite, two-mica granite, and granodiorite, are mostly distributed along the axis of the orogenic belt. Most of the granitoids are metaluminous or weakly peraluminous calc-alkaline granites[23,29−33], but some peraluminous high-K, calc-alkaline granites occur at Hanasi in the northwest and Qinghe in the southeast. Precise zircon dating indicates that these granitoids were mostly emplaced at 360−460 Ma[23,24,30,31,33,34]. In addition, high Mg-andesite and Nd-enriched basalts occur in the Devonian Aletai Formation in the southern margin of the Chinese Altai[35,36].

We separated abundant zircons from the Habahe sedimentary rocks, the paragneisses, and the Paleozoic granitoids. The zircons from the granitoids are clearly igneous in origin, whereas those from the sedimentary and gneissic rocks have several different morphologies, which imply different origins: (1) rounded zircon grains with oscillatory zoning and overgrowth rims (Figure 2(a)), which are interpreted as long-transported detrital zircon derived from an igneous source; (2) angular zircon fragment with oscillatory zoning and overgrowth rims (Figure 2(b)), which we consider to be volcanic in origin, related to nearby eruptions; and (3) euhedral zircons with oscillatory zoning, some of which have thin overgrowth rims (Figure 2(c)), possibly also magmatic in origin. We carried out a systematic U-Pb and Hf isotopic study of the recovered grains, taking care to analyze spots away from the overgrowth rims. These zircons have different ages, which reflect various stages of magmatic activity, and their Hf isotopic compositions reflect different magma sources. Therefore, the zircon U-Pb and Hf isotopic compositions can be used to unravel the magmatic evolutionary history of the region and the tectonic mechanisms responsible for the evolution.

2 Zircon U-Pb ages

2.1 Granitoids

J2-1: a gneissic biotite granite. Fifty-seven zircons were analyzed, 48 of which gave $^{206}Pb/^{238}U$ ages between 443 and 487 Ma, with a weighted mean of 466±3 Ma (Table 1, Figure 3(a)) representing the emplacement age. The other 9 grains are xenocrysts with $^{206}Pb/^{238}U$ ages between 495 and 585 Ma. The coeval granitoids are all highly deformed rocks that crop out mainly along the southern margin of the Chinese Altai[23,24,30,37].

Bu6-1: a gneissic biotite granite. Thirty-one zircon grains were analyzed, 27 of which gave $^{206}Pb/^{238}U$ ages between 390 and 441 Ma, with a weighted mean of 415±5 Ma (Table 1, Figure 3(b)) representing the emplacement age. These rocks are the dominant granitic phase in the region and are widely distributed in the Chinese Altai[23,24,30]. The other four zircons have older $^{206}Pb/^{238}U$ ages of 454, 473, 474 and 490 Ma and record an earlier stage of magmatic activity, probably represented by sample J2-1.

ARJ12: a gneissic biotite granite. Twenty-five zircon grains were analyzed, two of which gave Precambrian ages. The other 23 grains have $^{206}Pb/^{238}U$ ages between 360 and 407 Ma, with a weighted mean of 378±6 Ma (Table1, Figure 3(c)), representing the emplacement age. Ophiolites and mafic intrusions with similar ages also occur in the region[30,31,38,39].

CH15-7: a gneissic two-mica granite. Thirty-two zircons were analyzed, 10 of which gave $^{206}Pb/^{238}U$ ages between 349 and 361 Ma, with a weighted mean of 355±5 Ma (Table1, Figure 3(d)), representing the emplacement age. This age is similar to that of the Habahe granitic pluton in the western Chinese Altai[23]. Numerous inherited zircon grains in this sample have Paleozoic $^{206}Pb/^{238}U$ ages, mainly between 402 and 447 Ma. A few inherited grains have slightly older $^{206}Pb/^{238}U$ ages of 463−542 Ma (Table 1).
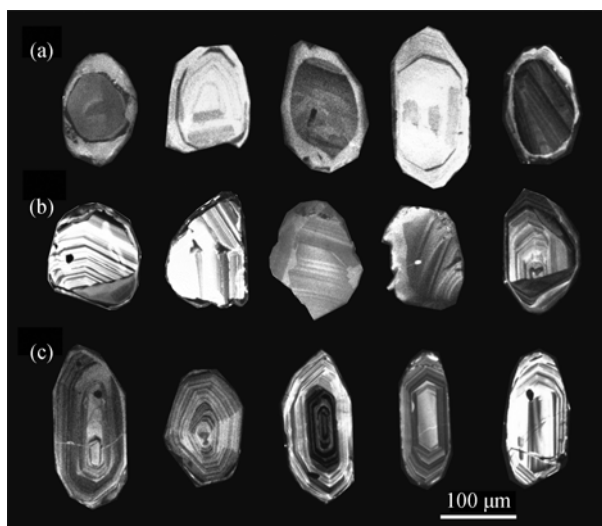
Figure 2 Representative CL images for zircon grains of the samples.
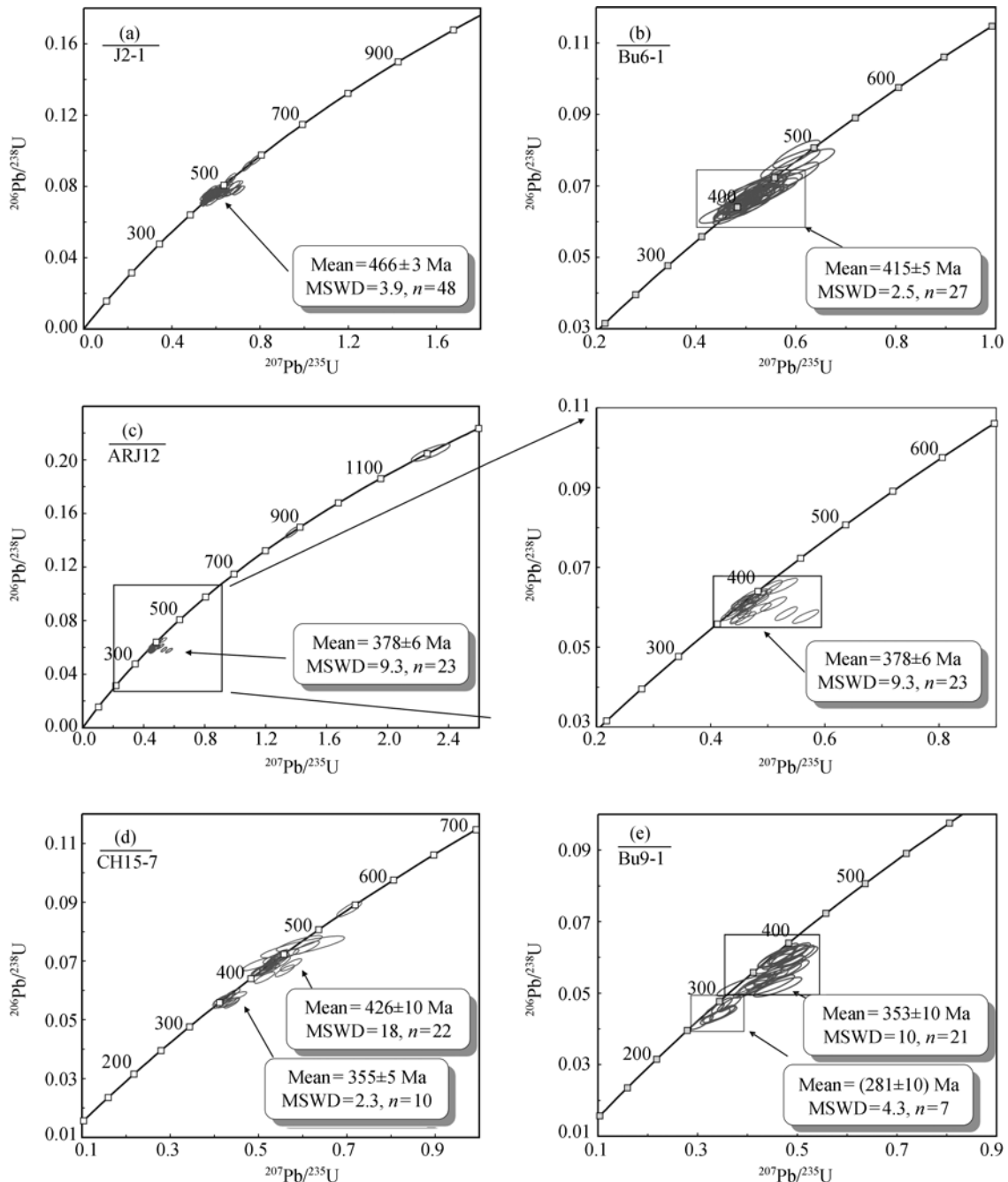
Figure 3 U-Pb concordia diagrams of zircon samples in the Chinese Altai.

Bu9-1: a pegmatitic dike. Twenty-eight zircons were analyzed, 7 of which gave $^{206}Pb/^{238}U$ ages between 264 and 296 Ma, with a weighted mean of 281±10 Ma (Table1, Figure 3(e)), representing the emplacement age. Coeval pegmatitic dikes are widely distributed in the Chinese Altai and host multi-metal mineral deposits of various sizes[23,40]. Other zircon grains from this sample have $^{206}Pb/^{238}U$ ages between 322 and 382 Ma, with a weighted mean of 353±10 Ma (Table 1, Figure 3(e)),

and these are considered to be the products of an earlier magmatic event (such as the one that produced sample CH15-7). Coeval granites have also been reported in the region[23,30].

2.2 Sedimentary rocks

We collected samples from the Habahe clastic sedimentary rocks and analyzed many detrital zircons. Most of the analyzed grains have ages of 460−540 Ma, with an

Table 1 U-Pb data of the granites in the Chinese Altai[a)]

Sample spot	Ratio						Age (Ma)						Disc%
	Pb^{207}/Pb^{206}	1σ	Pb^{207}/U^{235}	1σ	Pb^{206}/U^{238}	1σ	Pb^{207}/Pb^{206}	1σ	Pb^{206}/U^{238}	1σ	Pb^{207}/U^{235}	1σ	
J2-1	48°26′19.7″N, 87°17′51.8″E												
1	0.05535	0.00076	0.55889	0.00850	0.07322	0.00093	426	30	451	6	456	6	−7
2	0.05521	0.00078	0.55651	0.00860	0.07309	0.00093	420	31	449	6	455	6	−8
3	0.05551	0.00078	0.60063	0.00924	0.07845	0.00100	433	30	478	6	487	6	−13
4	0.05670	0.00079	0.59687	0.00909	0.07632	0.00097	479	31	475	6	474	6	1
5	0.05858	0.00078	0.61204	0.00908	0.07575	0.00096	552	29	485	6	471	6	15
6	0.05604	0.00083	0.56061	0.00903	0.07253	0.00093	454	32	452	6	451	6	1
7	0.05635	0.00082	0.58081	0.00916	0.07474	0.00096	465	32	465	6	465	6	0
8	0.05588	0.00111	0.58192	0.01198	0.07550	0.00100	447	43	466	8	469	6	−5
9	0.05644	0.00198	0.58802	0.02047	0.07555	0.00113	469	76	470	13	470	7	0
10	0.05997	0.00117	0.62847	0.01269	0.07599	0.00101	602	42	495	8	472	6	22
11	0.06275	0.00142	0.66443	0.01529	0.07678	0.00104	700	47	517	9	477	6	32
12	0.05882	0.00109	0.58027	0.01122	0.07153	0.00094	560	40	465	7	445	6	21
13	0.05697	0.00086	0.58296	0.00952	0.07420	0.00095	490	33	466	6	461	6	6
14	0.05395	0.00111	0.56757	0.01211	0.07629	0.00101	369	46	456	8	474	6	−29
15	0.05351	0.00082	0.55000	0.00908	0.07452	0.00096	351	34	445	6	463	6	−32
16	0.05598	0.00103	0.56560	0.01093	0.07326	0.00096	451	40	455	7	456	6	−1
17	0.05546	0.00081	0.56278	0.00896	0.07358	0.00094	431	32	453	6	458	6	−6
18	0.05798	0.00073	0.58919	0.00833	0.07368	0.00093	529	28	470	5	458	6	13
19	0.05669	0.00080	0.56237	0.00865	0.07193	0.00092	479	31	453	6	448	6	6
20	0.05513	0.00112	0.56931	0.01194	0.07488	0.00099	417	44	458	8	466	6	−12
21	0.05596	0.00089	0.55945	0.00949	0.07249	0.00093	450	34	451	6	451	6	0
22	0.05595	0.00067	0.57697	0.00791	0.07477	0.00094	450	26	463	5	465	6	−3
23	0.05552	0.00101	0.55421	0.01061	0.07238	0.00095	433	40	448	7	451	6	−4
24	0.06092	0.00111	0.63173	0.01208	0.07519	0.00099	636	39	497	8	467	6	27
25	0.05557	0.00069	0.59077	0.00828	0.07709	0.00098	435	27	471	5	479	6	−10
26	0.05626	0.00094	0.56413	0.01004	0.07270	0.00094	462	37	454	7	452	6	2
27	0.05648	0.00078	0.59044	0.00895	0.07580	0.00097	471	30	471	6	471	6	0
28	0.05943	0.00130	0.62623	0.01407	0.07641	0.00103	583	47	494	9	475	6	19
29	0.05820	0.00073	0.60683	0.00854	0.07560	0.00096	537	28	482	5	470	6	12
30	0.05672	0.00074	0.55601	0.00818	0.07114	0.00092	480	29	449	5	443	6	8
31	0.05574	0.00063	0.56629	0.00751	0.07371	0.00095	442	24	456	5	459	6	−4
32	0.06568	0.00092	0.70322	0.01092	0.07769	0.00102	796	29	541	7	482	6	39
33	0.06153	0.00086	0.68293	0.01056	0.08054	0.00105	658	30	529	6	499	6	24
34	0.05910	0.00089	0.64953	0.01072	0.07975	0.00105	571	33	508	7	495	6	13
35	0.05650	0.00079	0.60263	0.00932	0.07740	0.00101	471	31	479	6	481	6	−2
36	0.05401	0.00086	0.57875	0.01001	0.07775	0.00102	372	36	464	6	483	6	−30
37	0.05729	0.00098	0.63431	0.01157	0.08034	0.00106	502	37	499	7	498	6	1
38	0.05656	0.00093	0.59096	0.01047	0.07581	0.00100	474	36	472	7	471	6	1
39	0.05497	0.00119	0.57669	0.01289	0.07613	0.00104	411	47	462	8	473	6	−15
40	0.05756	0.00072	0.65433	0.00937	0.08249	0.00107	513	27	511	6	511	6	0
41	0.06405	0.00084	0.68809	0.01021	0.07796	0.00101	743	28	532	6	484	6	35
42	0.05606	0.00091	0.57927	0.01016	0.07498	0.00099	454	35	464	7	466	6	−3
43	0.05684	0.00120	0.61384	0.01339	0.07836	0.00107	485	46	486	8	486	6	0
44	0.05888	0.00067	0.74256	0.00990	0.09151	0.00118	563	25	564	6	565	7	0
45	0.05775	0.00088	0.66024	0.01101	0.08296	0.00109	520	33	515	7	514	6	1
46	0.05714	0.00074	0.66612	0.00973	0.08459	0.00110	497	28	518	6	524	7	−5
47	0.06118	0.00166	0.67639	0.01855	0.08022	0.00115	646	57	525	11	498	7	23
48	0.06346	0.00131	0.67442	0.01441	0.07711	0.00105	724	43	523	9	479	6	34
49	0.05635	0.00140	0.59563	0.01507	0.07670	0.00107	466	55	475	10	476	6	−2
50	0.05957	0.00082	0.77912	0.01193	0.09491	0.00124	588	30	585	7	585	7	1
51	0.05473	0.00104	0.57647	0.01146	0.07643	0.00102	401	42	462	7	475	6	−18
52	0.05655	0.00109	0.59093	0.01189	0.07583	0.00102	473	42	472	8	471	6	0
53	0.05635	0.00082	0.58268	0.00933	0.07503	0.00098	465	32	466	6	466	6	0

Sample spot	Ratio						Age (Ma)						Disc%
	Pb^{207}/Pb^{206}	1σ	Pb^{207}/U^{235}	1σ	Pb^{206}/U^{238}	1σ	Pb^{207}/Pb^{206}	1σ	Pb^{206}/U^{238}	1σ	Pb^{207}/U^{235}	1σ	
54	0.05582	0.00076	0.58064	0.00880	0.07547	0.00098	445	29	465	6	469	6	−5
55	0.05637	0.00091	0.58629	0.01022	0.07548	0.00099	466	36	469	7	469	6	−1
56	0.05605	0.00074	0.56471	0.00839	0.07311	0.00095	454	29	455	5	455	6	0
57	0.05588	0.00075	0.55274	0.00836	0.07178	0.00093	447	29	447	5	447	6	0
Bu6-1	48°03′17.8″N, 87°00′12.0″E												
1	0.05568	0.00140	0.53867	0.01276	0.07016	0.00134	440	55	438	8	437	8	1
2	0.05557	0.00196	0.51774	0.01748	0.06757	0.00138	435	77	424	12	421	8	3
3	0.05546	0.00206	0.54185	0.01932	0.07086	0.00148	431	81	440	13	441	9	−2
4	0.05601	0.00166	0.52105	0.01470	0.06748	0.00132	453	64	426	10	421	8	7
5	0.05463	0.00342	0.47748	0.02896	0.06340	0.00156	397	135	396	20	396	9	0
6	0.05823	0.00242	0.55037	0.02196	0.06855	0.00148	538	88	445	14	427	9	21
7	0.05739	0.00178	0.53755	0.01578	0.06794	0.00134	507	67	437	10	424	8	16
8	0.05457	0.00198	0.49107	0.01704	0.06527	0.00134	395	79	406	12	408	8	−3
9	0.05512	0.00224	0.50835	0.01976	0.06690	0.00142	417	88	417	13	417	9	0
10	0.05755	0.00208	0.53118	0.01840	0.06696	0.00138	513	78	433	12	418	8	19
11	0.05481	0.00268	0.51717	0.02432	0.06844	0.00154	404	106	423	16	427	9	−6
12	0.05705	0.00170	0.52330	0.01466	0.06654	0.00130	493	64	427	10	415	8	16
13	0.05508	0.00194	0.50304	0.01676	0.06625	0.00136	415	77	414	11	414	8	0
14	0.05500	0.00180	0.49982	0.01556	0.06593	0.00132	412	72	412	10	412	8	0
15	0.05665	0.00224	0.49963	0.01876	0.06398	0.00134	478	85	411	13	400	8	16
16	0.05550	0.00378	0.52830	0.03476	0.06905	0.00184	432	145	431	23	430	11	0
17	0.05656	0.00186	0.54196	0.01670	0.06951	0.00140	474	71	440	11	433	8	9
18	0.05545	0.00182	0.49626	0.01522	0.06492	0.00130	430	72	409	10	405	8	6
19	0.05613	0.00328	0.51412	0.02876	0.06643	0.00164	458	125	421	19	415	10	9
20	0.05512	0.00224	0.48785	0.01882	0.06420	0.00138	417	88	403	13	401	8	4
21	0.05509	0.00202	0.47415	0.01628	0.06242	0.00130	416	80	394	11	390	8	6
22	0.05388	0.00232	0.51220	0.02092	0.06894	0.00150	366	94	420	14	430	9	−17
23	0.05504	0.00224	0.48111	0.01846	0.06339	0.00136	414	88	399	13	396	8	4
24	0.05609	0.00314	0.51024	0.02722	0.06597	0.00160	456	120	419	18	412	10	10
25	0.05522	0.00220	0.51766	0.01940	0.06798	0.00146	421	87	424	13	424	9	−1
26	0.05576	0.00238	0.50243	0.02014	0.06533	0.00144	443	92	413	14	408	9	8
27	0.05415	0.00202	0.47482	0.01642	0.06358	0.00134	377	82	395	11	397	8	−5
28	0.05961	0.00192	0.60031	0.01852	0.07304	0.00146	589	68	477	12	454	9	23
29	0.05823	0.00264	0.61175	0.02674	0.07620	0.00170	538	96	485	17	473	10	12
30	0.05528	0.00188	0.60128	0.01916	0.07890	0.00160	424	74	478	12	490	10	−16
31	0.05602	0.00242	0.58893	0.02430	0.07625	0.00168	453	93	470	15	474	10	−5
ARJ12	47°29′08.1″N, 89°14′21.1″E												
1	0.05647	0.00074	0.45021	0.00626	0.05782	0.00067	470	29	377	4	362	4	23
2	0.05706	0.00092	0.45235	0.00750	0.05750	0.00068	493	35	379	5	360	4	27
3	0.05422	0.00075	0.45332	0.00660	0.06064	0.00071	380	31	380	5	380	4	0
4	0.06832	0.00089	1.37568	0.01907	0.14604	0.00170	878	27	879	8	879	10	0
5	0.07125	0.00116	0.56640	0.00950	0.05765	0.00069	965	33	456	6	361	4	63
6	0.05433	0.00091	0.45592	0.00784	0.06086	0.00072	385	37	381	5	381	4	1
7	0.05561	0.00081	0.46733	0.00711	0.06095	0.00072	437	32	389	5	381	4	13
8	0.08056	0.00184	2.28188	0.05212	0.20543	0.00267	1211	44	1207	16	1204	14	1
9	0.05631	0.00099	0.50356	0.00901	0.06486	0.00078	464	39	414	6	405	5	13
10	0.05575	0.00079	0.46725	0.00692	0.06079	0.00071	442	31	389	5	380	4	14
11	0.06610	0.00096	0.53232	0.00802	0.05840	0.00069	810	30	433	5	366	4	55
12	0.05453	0.00108	0.43918	0.00878	0.05842	0.00071	393	43	370	6	366	4	7
13	0.06084	0.00109	0.51024	0.00931	0.06082	0.00073	634	38	419	6	381	4	40
14	0.05640	0.00076	0.46388	0.00657	0.05965	0.00070	467	30	387	5	374	4	20
15	0.05426	0.00121	0.46166	0.01036	0.06171	0.00077	382	49	385	7	386	5	−1
16	0.05562	0.00083	0.48175	0.00747	0.06282	0.00074	437	32	399	5	393	4	10

Sample spot	Ratio						Age (Ma)						Disc%
	Pb^{207}/Pb^{206}	1σ	Pb^{207}/U^{235}	1σ	Pb^{206}/U^{238}	1σ	Pb^{207}/Pb^{206}	1σ	Pb^{206}/U^{238}	1σ	Pb^{207}/U^{235}	1σ	
17	0.05848	0.00149	0.47706	0.01208	0.05916	0.00076	548	55	396	8	371	5	32
18	0.05401	0.00074	0.44112	0.00635	0.05924	0.00069	371	31	371	4	371	4	0
19	0.05635	0.00095	0.48700	0.00838	0.06268	0.00075	465	37	403	6	392	5	16
20	0.05430	0.00114	0.46008	0.00978	0.06145	0.00076	383	47	384	7	385	5	0
21	0.05615	0.00131	0.47485	0.01112	0.06133	0.00077	458	51	395	8	384	5	16
22	0.05426	0.00100	0.46885	0.00880	0.06267	0.00076	382	41	390	6	392	5	−3
23	0.05821	0.00127	0.52394	0.01152	0.06528	0.00081	537	48	428	8	408	5	24
24	0.05543	0.00113	0.47522	0.00981	0.06218	0.00076	429	44	395	7	389	5	9
25	0.05846	0.00089	0.46136	0.00731	0.05724	0.00068	547	33	385	5	359	4	34
CH15-7	47°54′22.1″N, 87°38′58.4″E												
1	0.05509	0.00076	0.52279	0.00768	0.06885	0.00082	416	30	427	5	429	5	−3
2	0.05582	0.00172	0.55062	0.01677	0.07157	0.00098	445	67	445	11	446	6	0
3	0.05559	0.00103	0.52617	0.00997	0.06868	0.00085	436	40	429	7	428	5	2
4	0.05840	0.00093	0.70570	0.01167	0.08767	0.00107	545	34	542	7	542	6	1
5	0.05515	0.00124	0.51119	0.01154	0.06726	0.00086	418	49	419	8	420	5	0
6	0.05532	0.00084	0.52284	0.00833	0.06858	0.00083	425	33	427	6	428	5	−1
7	0.05577	0.00115	0.54198	0.01134	0.07052	0.00089	443	45	440	7	439	5	1
8	0.05540	0.00173	0.43995	0.01357	0.05762	0.00079	428	68	370	10	361	5	16
9	0.05658	0.00207	0.59232	0.02140	0.07597	0.00111	474	80	472	14	472	7	0
10	0.05654	0.00113	0.52236	0.01061	0.06704	0.00084	473	44	427	7	418	5	12
11	0.05335	0.00113	0.41941	0.00900	0.05704	0.00072	344	47	356	6	358	4	−4
12	0.05255	0.00158	0.49965	0.01489	0.06899	0.00094	310	67	412	10	430	6	−39
13	0.05733	0.00086	0.43917	0.00690	0.05559	0.00067	504	33	370	5	349	4	31
14	0.05438	0.00081	0.42784	0.00665	0.05709	0.00069	387	33	362	5	358	4	7
15	0.05425	0.00096	0.41537	0.00751	0.05556	0.00068	381	39	353	5	349	4	9
16	0.05388	0.00100	0.42691	0.00813	0.05749	0.00071	366	42	361	6	360	4	2
17	0.05744	0.00091	0.54975	0.00909	0.06944	0.00084	508	35	445	6	433	5	15
18	0.05520	0.00082	0.54608	0.00853	0.07178	0.00087	420	33	442	6	447	5	−6
19	0.05543	0.00109	0.51294	0.01028	0.06714	0.00084	430	43	420	7	419	5	2
20	0.05926	0.00117	0.60844	0.01219	0.07450	0.00093	577	42	483	8	463	6	20
21	0.05501	0.00103	0.50646	0.00971	0.06681	0.00083	413	41	416	7	417	5	−1
22	0.06087	0.00094	0.55928	0.00901	0.06667	0.00081	635	33	451	6	416	5	34
23	0.05822	0.00387	0.59989	0.03891	0.07477	0.00151	537	140	477	25	465	9	13
24	0.05300	0.00079	0.41182	0.00642	0.05638	0.00068	329	33	350	5	354	4	−7
25	0.05541	0.00097	0.54085	0.00971	0.07083	0.00087	428	38	439	6	441	5	−3
26	0.05792	0.00105	0.51377	0.00955	0.06436	0.00079	527	40	421	6	402	5	24
27	0.05669	0.00071	0.55078	0.00745	0.07049	0.00084	479	28	446	5	439	5	8
28	0.05433	0.00089	0.44032	0.00744	0.05881	0.00071	385	36	371	5	368	4	4
29	0.06056	0.00104	0.57338	0.01009	0.06870	0.00084	624	36	460	7	428	5	31
30	0.05655	0.00112	0.43605	0.00879	0.05595	0.00070	473	44	368	6	351	4	26
31	0.05559	0.00127	0.51199	0.01176	0.06683	0.00085	436	50	420	8	417	5	4
32	0.05560	0.00121	0.42740	0.00938	0.05577	0.00071	436	47	361	7	350	4	20
Bu9-1	48°03′48.1″N, 87°00′16.3″E												
1	0.05686	0.00246	0.34487	0.01394	0.04400	0.00092	486	93	301	10	278	6	43
2	0.05711	0.00190	0.35045	0.01056	0.04452	0.00086	496	72	305	8	281	5	43
3	0.05361	0.00168	0.30919	0.00918	0.04183	0.00082	355	69	274	7	264	5	26
4	0.05435	0.00142	0.34882	0.00852	0.04655	0.00088	386	58	304	6	293	5	24
5	0.05339	0.00148	0.33288	0.00854	0.04523	0.00086	345	62	292	6	285	5	17
6	0.05618	0.00164	0.36328	0.00978	0.04691	0.00088	459	63	315	7	296	5	36
7	0.05601	0.00218	0.33548	0.01226	0.04345	0.00088	453	84	294	9	274	5	39
8	0.05706	0.00192	0.41096	0.01270	0.05224	0.00102	494	73	350	9	328	6	34
9	0.05757	0.00214	0.40604	0.01400	0.05116	0.00102	513	80	346	10	322	6	37
10	0.05491	0.00334	0.39533	0.02308	0.05221	0.00126	409	131	338	17	328	8	20

(*Continued*)

Sample spot	Ratio						Age (Ma)						Disc%
	Pb^{207}/Pb^{206}	1σ	Pb^{207}/U^{235}	1σ	Pb^{206}/U^{238}	1σ	Pb^{207}/Pb^{206}	1σ	Pb^{206}/U^{238}	1σ	Pb^{207}/U^{235}	1σ	
11	0.05788	0.00200	0.41504	0.01358	0.05200	0.00104	525	74	352	10	327	6	38
12	0.05914	0.00250	0.43914	0.01768	0.05385	0.00114	572	89	370	12	338	7	41
13	0.05862	0.00160	0.44119	0.01130	0.05459	0.00104	553	58	371	8	343	6	38
14	0.06194	0.00288	0.44642	0.01974	0.05228	0.00114	672	96	375	14	329	7	51
15	0.06013	0.00274	0.45951	0.01992	0.05544	0.00120	608	96	384	14	348	7	43
16	0.06464	0.00294	0.46062	0.01986	0.05169	0.00112	763	93	385	14	325	7	57
17	0.05950	0.00210	0.47444	0.01564	0.05784	0.00114	585	75	394	11	362	7	38
18	0.05653	0.00182	0.46313	0.01362	0.05943	0.00114	473	70	386	9	372	7	21
19	0.05673	0.00264	0.47053	0.02054	0.06017	0.00128	481	100	392	14	377	8	22
20	0.05536	0.00202	0.45870	0.01522	0.06011	0.00118	427	79	383	11	376	7	12
21	0.05747	0.00228	0.48358	0.01768	0.06104	0.00122	510	85	401	12	382	7	25
22	0.06222	0.00222	0.48393	0.01632	0.05641	0.00114	682	74	401	11	354	7	48
23	0.05815	0.00200	0.48534	0.01576	0.06054	0.00120	535	74	402	11	379	7	29
24	0.06049	0.00212	0.50103	0.01650	0.06008	0.00120	621	74	412	11	376	7	39
25	0.05615	0.00152	0.47304	0.01192	0.06111	0.00116	458	59	393	8	382	7	17
26	0.05643	0.00202	0.45297	0.01534	0.05823	0.00116	469	77	379	11	365	7	22
27	0.05997	0.00226	0.47579	0.01696	0.05755	0.00116	602	80	395	12	361	7	40
28	0.06008	0.00174	0.50145	0.01354	0.06054	0.00116	606	61	413	9	379	7	38

a) Disc%=[1–($^{206}Pb/^{238}U$ Age)/($^{207}Pb/^{206}Pb$ Age)]×100. The analyses methods are from refs. [21, 24].

age peak at 505 Ma. A few zircons have Proterozoic ages (~776－826 Ma) or Archean ages[41] (Figure 4(a)).
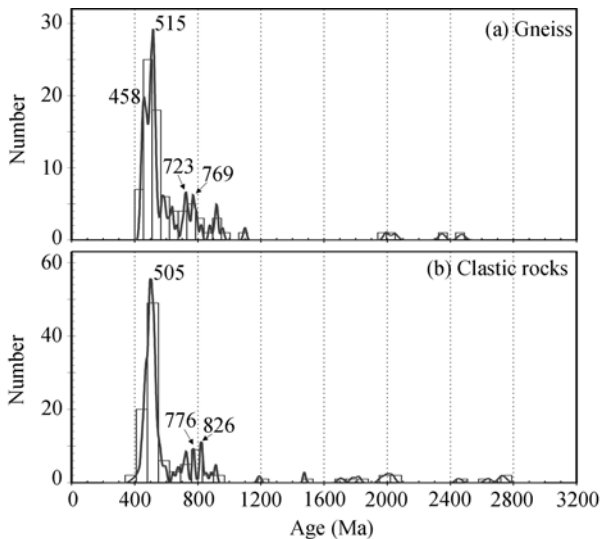
Figure 4 Age distribution plots of detrital zircons from sedimentary rocks and gneisses in the Chinese Altai. Data are from Sun et al.[24] and Yuan et al.[41].

2.3 Gneiss

We collected high-grade gneissic rocks from the Chonghuer and Hanasi areas. Petrological and geo-chemical data show that these rocks are paragneisses[24]. We analyzed zircons of non-metamorphic origin, and found that most have ages of ~515 Ma. A smaller number of grains have Neoproterozoic ages (723－769

Ma) and these are accompanied by sparse grains of Paleoproterozoic and Archean age[24] (Figure 4(b)).

3 Zircon Hf isotopic data

We analyzed Lu-Hf isotopic compositions for a suite of representative zircons from the samples described above and calculated the initial $\varepsilon_{Hf}(t)$ values based on the U-Pb ages of individual grains (the $^{207}Pb/^{206}Pb$ age was used for those grains with ages >1000 Ma, and $^{206}Pb/^{238}U$ age was used for those <1000 Ma). The results are presented in Table 2 (data for sedimentary and gneissic rocks are in references[22,24]). The diagram of zircon U-Pb age vs. $\varepsilon_{Hf}(t)$ value shows an abrupt change of Hf isotopic composition at ~420 Ma (Figure 5). Before this time the
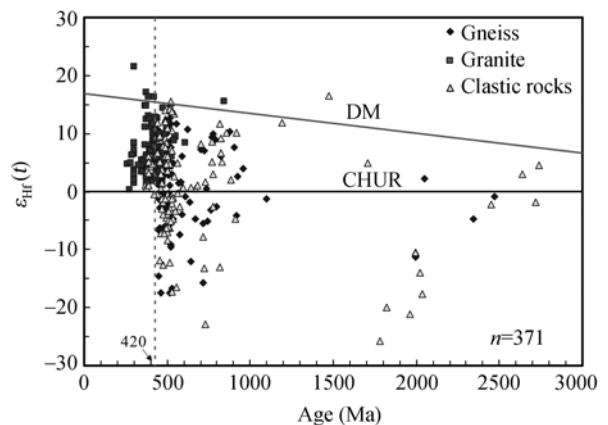
Figure 5 Diagrams of $\varepsilon_{Hf}(t)$ values vs. crystallizing ages for zircons from granites, gneisses and sedimentary rocks in the Chinese Altai. Data are from Long et al.[21] and Sun et al.[24].

Table 2 Hf isotope data of the granites in the Chinese Altai

Sample	^{176}Yb/^{177}Hf	2σ	^{176}Lu/^{177}Hf	2σ	^{176}Hf/^{177}Hf	2σ	Age (Ma)	(^{176}Hf/^{177}Hf)$_i$	$\varepsilon_{Hf}(t)$	T_{DM}^{c}	$f_{Lu/Hf}$
J2-1											
1	0.071640	0.002850	0.001916	0.000051	0.282653	0.000045	466	0.282636	5.44	871	−0.94
2	0.058181	0.001664	0.001605	0.000052	0.282705	0.000025	466	0.282691	7.38	789	−0.95
3	0.090828	0.001188	0.002846	0.000043	0.282644	0.000018	466	0.282619	4.83	907	−0.91
4	0.089544	0.001117	0.002406	0.000029	0.282656	0.000021	466	0.282635	5.41	878	−0.93
5	0.070743	0.000525	0.002219	0.000009	0.282668	0.000014	466	0.282649	5.91	855	−0.93
6	0.053453	0.000430	0.001428	0.000018	0.282580	0.000022	514	0.282566	4.03	963	−0.96
7	0.080063	0.005343	0.002138	0.000115	0.282692	0.000027	466	0.282673	6.77	819	−0.94
8	0.049945	0.000562	0.001513	0.000015	0.282630	0.000022	511	0.282615	5.71	894	−0.95
9	0.062173	0.001608	0.001662	0.000036	0.282791	0.000032	498	0.282775	11.08	666	−0.95
10	0.057400	0.001307	0.001488	0.000019	0.282702	0.000019	466	0.282689	7.31	791	−0.96
11	0.054428	0.000476	0.001466	0.000026	0.282648	0.000022	466	0.282635	5.41	867	−0.96
12	0.055773	0.000779	0.001530	0.000030	0.282689	0.000030	495	0.282675	7.46	810	−0.95
13	0.082948	0.005732	0.002019	0.000112	0.282610	0.000022	466	0.282592	3.90	935	−0.94
14	0.052767	0.000560	0.001396	0.000025	0.282633	0.000022	466	0.282621	4.90	887	−0.96
15	0.062096	0.000605	0.001643	0.000013	0.282685	0.000018	466	0.282670	6.66	818	−0.95
16	0.039684	0.000441	0.001002	0.000009	0.282635	0.000021	466	0.282626	5.09	875	−0.97
17	0.092443	0.001074	0.002311	0.000021	0.282657	0.000019	466	0.282637	5.48	874	−0.93
18	0.031585	0.000693	0.000909	0.000029	0.282680	0.000026	466	0.282672	6.71	809	−0.97
19	0.060805	0.001144	0.001591	0.000034	0.282655	0.000020	466	0.282641	5.63	860	−0.95
20	0.048428	0.002672	0.001657	0.000098	0.282772	0.000030	466	0.282757	9.73	694	−0.95
BU6-1											
1	0.037871	0.000920	0.001448	0.000032	0.282678	0.000040	415	0.282667	5.41	824	−0.96
2	0.038993	0.001443	0.001480	0.000051	0.282774	0.000039	415	0.282763	8.81	686	−0.96
3	0.020245	0.001463	0.000844	0.000064	0.282755	0.000039	415	0.282749	8.31	702	−0.97
4	0.066652	0.001885	0.002459	0.000068	0.282771	0.000037	415	0.282752	8.42	710	−0.93
5	0.032394	0.006139	0.001045	0.000179	0.282684	0.000080	473	0.282675	6.99	806	−0.97
6	0.033130	0.002615	0.001153	0.000088	0.282781	0.000045	415	0.282772	9.15	670	−0.97
7	0.032878	0.001716	0.001235	0.000062	0.282886	0.000038	415	0.282877	12.84	522	−0.96
8	0.031838	0.002319	0.001189	0.000083	0.282754	0.000028	415	0.282745	8.17	710	−0.96
9	0.051572	0.000934	0.001890	0.000037	0.282882	0.000049	415	0.282867	12.51	537	−0.94
10	0.034411	0.002750	0.001262	0.000096	0.282621	0.000037	415	0.282611	3.43	901	−0.96
11	0.062339	0.000381	0.002207	0.000010	0.282778	0.000048	415	0.282761	8.75	694	−0.93
12	0.018386	0.000271	0.000796	0.000012	0.282799	0.000041	415	0.282793	9.87	639	−0.98
13	0.040762	0.002683	0.001493	0.000094	0.282813	0.000038	415	0.282801	10.17	631	−0.96
14	0.079068	0.000831	0.002565	0.000019	0.282861	0.000053	415	0.282841	11.56	580	−0.92
15	0.047799	0.000351	0.001725	0.000009	0.282845	0.000047	415	0.282831	11.23	589	−0.95
16	0.028222	0.002348	0.001035	0.000083	0.282757	0.000033	490	0.282747	9.90	703	−0.97
17	0.043451	0.001094	0.001666	0.000039	0.282899	0.000041	474	0.282885	14.41	509	−0.95
18	0.050417	0.000421	0.001467	0.000004	0.282856	0.000029	415	0.282845	11.70	569	−0.96
19	0.147638	0.000400	0.004428	0.000015	0.282837	0.000055	415	0.282803	10.21	648	−0.87
20	0.067066	0.001148	0.002096	0.000023	0.282744	0.000027	415	0.282728	7.57	742	−0.94
21	0.051531	0.001360	0.001859	0.000047	0.282689	0.000044	415	0.282675	5.70	816	−0.94
22	0.016956	0.001288	0.000598	0.000047	0.282725	0.000034	415	0.282721	7.32	739	−0.98
23	0.014225	0.000529	0.000533	0.000015	0.282734	0.000035	415	0.282730	7.65	725	−0.98
ARJ12											
1	0.043784	0.000219	0.001165	0.000015	0.282630	0.000016	378	0.282621	2.98	886	−0.96
2	0.036517	0.000226	0.000983	0.000005	0.282650	0.000015	378	0.282643	3.75	853	−0.97
3	0.036561	0.000084	0.001073	0.000011	0.282663	0.000016	378	0.282655	4.18	837	−0.97
4	0.043181	0.000884	0.001162	0.000028	0.282631	0.000015	378	0.282623	3.04	884	−0.97
5	0.044744	0.000272	0.001329	0.000011	0.282573	0.000017	378	0.282563	0.92	971	−0.96
6	0.043189	0.000948	0.001200	0.000022	0.282627	0.000015	378	0.282618	2.87	891	−0.96
7	0.031660	0.000068	0.000889	0.000003	0.282663	0.000015	378	0.282657	4.24	832	−0.97
8	0.062400	0.001241	0.001804	0.000036	0.282640	0.000015	378	0.282627	3.18	887	−0.95
9	0.043162	0.000469	0.001263	0.000017	0.282671	0.000018	378	0.282662	4.42	830	−0.96

Sample	^{176}Yb/^{177}Hf	2σ	^{176}Lu/^{177}Hf	2σ	^{176}Hf/^{177}Hf	2σ	Age (Ma)	(^{176}Hf/^{177}Hf)$_i$	$\varepsilon_{Hf}(t)$	T_{DM}^c	$f_{Lu/Hf}$
10	0.044758	0.000910	0.001301	0.000030	0.282630	0.000015	378	0.282620	2.95	889	−0.96
11	0.041611	0.000214	0.001247	0.000009	0.282632	0.000018	378	0.282623	3.05	885	−0.96
12	0.034270	0.000392	0.000959	0.000003	0.282629	0.000018	378	0.282622	3.00	883	−0.97
13	0.141080	0.012540	0.003181	0.000263	0.282643	0.000023	378	0.282620	2.94	917	−0.90
14	0.037222	0.000312	0.001096	0.000012	0.282646	0.000016	378	0.282638	3.58	861	−0.97
15	0.041462	0.000251	0.001220	0.000010	0.282635	0.000018	378	0.282626	3.16	880	−0.96
16	0.032711	0.000901	0.001012	0.000024	0.282712	0.000016	378	0.282704	5.92	767	−0.97
17	0.047599	0.000866	0.001484	0.000018	0.282617	0.000017	378	0.282606	2.44	912	−0.96
18	0.035278	0.000347	0.001068	0.000013	0.282640	0.000013	378	0.282632	3.37	869	−0.97
19	0.042668	0.000267	0.001247	0.000007	0.282639	0.000017	378	0.282631	3.31	874	−0.96
CH15-7											
1	0.075336	0.002780	0.002220	0.000070	0.282639	0.000033	429	0.282621	4.08	899	−0.93
2	0.057362	0.001970	0.001755	0.000061	0.282664	0.000029	355	0.282652	3.55	851	−0.95
3	0.050665	0.002833	0.001569	0.000082	0.282708	0.000029	446	0.282695	7.09	783	−0.95
4	0.064493	0.000944	0.001919	0.000023	0.282527	0.000027	472	0.282510	1.11	1053	−0.94
5	0.054269	0.002920	0.001704	0.000089	0.282716	0.000026	542	0.282699	9.36	774	−0.95
6	0.130511	0.007031	0.004028	0.000195	0.282685	0.000033	428	0.282653	5.20	874	−0.88
7	0.084225	0.001610	0.002731	0.000076	0.282696	0.000035	420	0.282674	5.77	827	−0.92
8	0.081383	0.003485	0.002570	0.000106	0.282711	0.000027	439	0.282690	6.77	800	−0.92
9	0.055556	0.002555	0.001936	0.000070	0.282689	0.000029	355	0.282676	4.41	819	−0.94
10	0.066378	0.002981	0.002144	0.000099	0.282622	0.000020	430	0.282604	3.53	921	−0.94
11	0.056749	0.002104	0.001675	0.000038	0.282663	0.000020	355	0.282652	3.55	850	−0.95
12	0.074118	0.004877	0.002304	0.000144	0.282705	0.000034	355	0.282690	4.90	803	−0.93
13	0.056090	0.001371	0.001751	0.000036	0.282647	0.000022	433	0.282633	4.62	874	−0.95
14	0.062237	0.002409	0.002036	0.000077	0.282674	0.000019	447	0.282657	5.76	843	−0.94
15	0.069833	0.003785	0.002294	0.000116	0.282641	0.000035	416	0.282623	3.87	897	−0.93
16	0.061638	0.001687	0.001988	0.000052	0.282697	0.000023	441	0.282680	6.46	808	−0.94
17	0.083013	0.004696	0.002678	0.000154	0.282599	0.000029	402	0.282579	2.01	968	−0.92
18	0.044193	0.002477	0.001445	0.000076	0.282680	0.000027	355	0.282670	4.20	821	−0.96
19	0.057628	0.002882	0.001909	0.000100	0.282655	0.000024	355	0.282642	3.21	867	−0.94
20	0.052654	0.000497	0.001349	0.000025	0.282684	0.000030	355	0.282675	4.36	814	−0.96
Bu9-1											
1	0.150092	0.005247	0.004131	0.000084	0.282790	0.000070	281	0.282769	6.05	715	−0.88
2	0.077752	0.001190	0.001732	0.000039	0.282638	0.000022	281	0.282629	1.10	888	−0.95
3	0.321791	0.010177	0.010161	0.000287	0.282752	0.000035	281	0.282698	3.56	938	−0.69
4	0.100005	0.003892	0.002910	0.000119	0.283212	0.000222	281	0.283196	21.19	58	−0.91
5	0.045542	0.001374	0.001131	0.000062	0.282792	0.000059	281	0.282786	6.68	655	−0.97
6	0.151579	0.005717	0.003762	0.000183	0.282683	0.000081	281	0.282664	2.34	870	−0.89
7	0.029441	0.003409	0.000925	0.000119	0.282687	0.000041	281	0.282682	2.99	800	−0.97
8	0.059223	0.001160	0.001402	0.000019	0.282635	0.000022	281	0.282628	1.07	884	−0.96
9	0.128982	0.005262	0.003308	0.000134	0.282667	0.000027	281	0.282650	1.84	883	−0.90
10	0.098691	0.007604	0.002977	0.000234	0.282668	0.000023	281	0.282652	1.93	874	−0.91
11	0.101214	0.004730	0.002257	0.000086	0.282658	0.000023	281	0.282646	1.72	871	−0.93
12	0.182665	0.017575	0.006180	0.000572	0.282850	0.000147	281	0.282818	7.79	661	−0.81
13	0.045969	0.002117	0.001538	0.000059	0.282678	0.000030	281	0.282670	2.57	825	−0.95
14	0.092882	0.003356	0.002220	0.000101	0.282837	0.000049	281	0.282826	8.07	608	−0.93
15	0.091381	0.006371	0.003167	0.000252	0.282788	0.000059	281	0.282772	6.16	698	−0.90
16	0.062971	0.002030	0.001889	0.000061	0.282706	0.000029	281	0.282696	3.48	793	−0.94
17	0.056298	0.001713	0.001902	0.000078	0.282752	0.000029	281	0.282742	5.10	727	−0.94
18	0.097221	0.001417	0.003111	0.000054	0.282656	0.000029	281	0.282639	1.47	896	−0.91
19	0.081629	0.000523	0.002483	0.000017	0.282725	0.000039	281	0.282712	4.03	779	−0.93
20	0.104679	0.005827	0.003479	0.000180	0.282641	0.000027	281	0.282622	0.88	927	−0.90
21	0.065834	0.001392	0.002151	0.000044	0.282619	0.000029	281	0.282608	0.36	925	−0.94
22	0.056600	0.001345	0.001975	0.000057	0.282749	0.000023	281	0.282738	4.99	733	−0.94

a) $T_{DM}{}^c = t + (1/\lambda) \times \ln[1+(({}^{176}\text{Hf}/{}^{177}\text{Hf})_{S,\,t} - ({}^{176}\text{Hf}/{}^{177}\text{Hf})_{DM,\,t})/(({}^{176}\text{Lu}/{}^{177}\text{Hf})_{UC} - ({}^{176}\text{Lu}/{}^{177}\text{Hf})_{DM})]$. Abbreviations: UC, upper crust; S, sample; DM, depleted mantle. The analyses methods are from refs. [21, 24].

$\varepsilon_{Hf}(t)$ values are both positive and negative, but after this time they are all negative.

4 Discussions

4.1 Geodynamic significance of the abrupt change in zircon Hf isotopic compositions

Because zircon can accommodate large quantities of Hf, but not its radioactive parent Lu, the Hf isotopic composition of zircon remains essentially constant after its formation. Thus, the Hf isotopic composition of igneous zircons can faithfully record that of the precursor magma. All the zircons in this study, including those from sedimentary rocks and paragneisses, are igneous in origin[22,24]. Because these zircons have ages between 280 Ma and 2800 Ma, their Hf isotopic compositions should reflect the characteristics of the parental magmas over a long evolutionary history. There is a clear change in the $\varepsilon_{Hf}(t)$ values of zircon from both positive and negative to only positive at ~420 Ma (Figure 5). This means that both ancient (represented by negative $\varepsilon_{Hf}(t)$ values) and juvenile materials (represented by positive $\varepsilon_{Hf}(t)$ values) existed in the magma source prior to ~420 Ma, but that juvenile material became dominant in the source after ~420 Ma. Because zircon mostly crystallizes in intermediate-silicic magmas that originated in the lithosphere, especially the middle-lower crust, this abrupt change in Hf isotopic compositions may reveal a dramatic change in the composition of the lithosphere. Beginning at ~420 Ma a large amount of juvenile material must have been added to the lithosphere, but none of the previously proposed tectonic models for the region can accommodate such a process. Therefore, we propose a new model involving ridge subduction to account for the dramatic change.

4.2 A ridge subduction model

In the ocean basins, newly formed crust routinely encounters subduction zones and is recycled back into the mantle. During this process, spreading oceanic ridges may collide with subduction zones and be carried beneath the overriding plate[42−44]. When a ridge is subducted, spreading can continue for some time and form a 'slab window' along the edges of the divergent slab. Hot asthenosphere will then rise through the slab window, causing a dramatic increase in the temperature of the overriding slab and the mantle wedge. The addition of heat to the system will lead to increasing of the geo-

thermal gradient, and form special characteristics of magmatic activity and metamorphism and sedimentation. The uplift of the hot asthenosphere will cause rifting of the overriding plate, generating a series of fore-arc or back-arc basins[45−47]. The thermal input will cause decompressional melting of the lithosphere and high temperature-low pressure metamorphism[48,49]. The melts formed by decompressional melting of the lithosphere will differ significantly from normal arc-type calk-alkaline rocks[50,51], and may produce adakites, high-Mg andesites and Nb-rich basalts[42,52−54](Figure 6). Therefore, the ridge subduction model can easily explain the rapid addition of huge amounts of juvenile material to the Chinese Altai, and can also account for the following geological phenomena:

(1) We recently found Early Paleozoic ophiolitic mélange in the Alegedaiyi area of the northwestern Chinese Altai. The mafic rocks possess a variety of geochemical types such as arc tholeiite, back-arc basalt, and enriched and transitional mid ocean ridge basalt[55]. In addition, the ophiolitic rocks in the Kuerti area are considered to be back-arc basin basalts that possess characteristics of both subduction zone and MORB[38], and these are associated with plagiogranite having a zircon SHRIMP age of 372±19 Ma[39]. Nearby mafic intrusions in the Habahe and Keketuohai areas have ages of 375±4.5 Ma[31] and 408±6 Ma[30], respectively. A ridge subduction setting is suitable for the formation of these magmatic associations with complex source characteristics.

(2) The abundant granitoids with ages of ~400 Ma in the Chinese Altai are mostly tonalite and granodiorite[23,24,30]. Geochemically, they straddle the boundary between low-K tholeiitic and high-K calc-alkaline rocks. Their positive $\varepsilon_{Hf}(t)$ values indicate that their precursor magmas mainly came from a juvenile source. The formation of granitoids on such a scale requires underplating by voluminous mafic magma and melting of juvenile materials. Ridge subduction can provide not only required heat, but also the juvenile material. We postulate that the source of these granitoids was juvenile material produced by early, normal subduction processes, including volcanic rocks and accretionary complexes dragged down to the middle-lower crustal level. These source rocks were partially melted when underplated and heated by the asthenosphere-derived magma rising through the slab window. There was a decline in the volume of typical calc-alkaline arc magmatism accom-

panied by an increase in high-Mg andesite and tholeiitic mafic magmatism at this time (~400 to ~370 Ma)[30,31,36,38], which may reflect a decrease in fluid-induced metasomatism after formation of the slab window[50,51].

(3) In the Xiaoerbulake and Ashele areas of the southern Chinese Altai, there is a magmatic association of adakite, boninite, high-Ti basalt, and Nb-rich basalt[36]. Similar petrological associations occur along the circum-Pacific subduction zones, such as in southwestern Japan, Alaska, Baja California, Costa Rica, and southern Chile, where they are considered to be genetically related to slab windows and ridge subduction[43,50].

(4) High-temperature, low-pressure metamorphism took place in the Early Paleozoic in the Chinese Altai. The metamorphic temperatures were mainly in the range of $500-750℃$ at pressures of $2-4$ kb, suggesting a metamorphic geotherm of $60-150℃/km$[56]. We analyzed zircon overgrowth rims from these metamorphic rocks and obtained an age of ~390 Ma[21]. We also applied the zircon Ti thermometer to the overgrowth rims and obtained temperature $≥710℃$, suggesting that the zircon rims formed at ~390 Ma during the high-T low-P metamorphism. Thus, the metamorphism may have been due to upwelling of the asthenosphere and opening of a slab window during ridge subduction.

High-T, low-P metamorphism is often accompanied by hydrothermal mineralization similar to that in the Chinese Altai. Pb model ages of $385-390$ Ma have been obtained for the multi-metal mineral deposits in the southern Chinese Altai, and their fluid inclusions have S and O isotopic compositions of $\delta^{34}S=-4.3‰$ and $\delta^{18}O$ >7‰. These isotopic characteristics are typical for deep
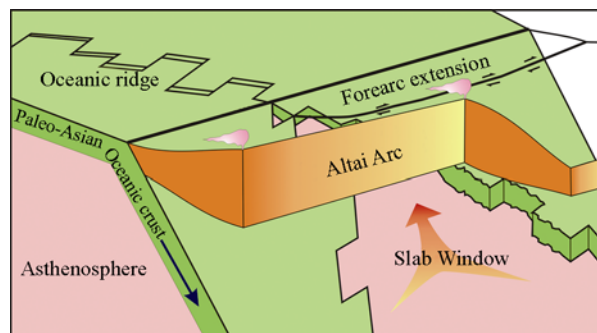
Figure 6 Tectonic model of ridge subduction in the Chinese Altai (modified from Thorkelson[51]).

level fluids[57] and are consistent with the ridge subduction model.

5 Conclusions

Hf isotopic data for zircons from granitoids, sedimentary rocks and gneisses from the Chinese Altai demonstrate that huge amounts of juvenile material were added to the lithosphere at ~420 Ma, which thoroughly modified its composition. We suggest that this dramatic change coincided with the initiation of ridge subduction in the region. The model can explain the formation of the igneous rocks in the period, such as the voluminous granitoids, mafic rocks with complicated compositions and an association of adakite-high-Mg andesite-boninite-high-Ti basalt-Nb-rich basalt, and coeval high-T-low-P metamorphism.

1 Faure G, Mensing T M. Isotopes: Principles and Applications. 3rd ed. John Wiley & Sons Press, 2005

2 He G Q, Han B F, Yue Y J, et al. Tectonic division and crustal evolution of Altay orogenic belt in China (in Chinese). Geosci Xinjiang, 1990, 2: 9−20

3 Windley B F, Kröner A, Guo J, et al. Neoproterozoic to Paleozoic geology of the Altai orogen, NW China: New zircon age data and tectonic evolution. J Geol, 2002, 110: 719−739[doi]

4 Chen F W, Li H Q, Wang D H, et al. New chronological evidence for Yanshanian diagenetic mineralization in China's Altay orogenic belt. Chin Sci Bull, 2000, 45(2): 108−114

5 Rui Z Y, Goldfarb R J, Qiu Y M, et al. Paleozoic ── Early Mesozoic gold deposits of the Xinjiang Autonomous Region, northwestern China. Miner Depos, 2002, 37(3-4): 393−418

6 Han B F, Ji J Q, Song B, et al. SHRIMP zircon U-Pb ages of kalatongke No. 1 and Huangshandong Cu-Ni-bearing mafic-ultramafic complexes, North Xinjiang, and geological implications. Chin Sci Bull, 2004, 49(22): 2424−2429

7 Yuan F, Zhou T F, Tan L G, et al. Geochemistry, geochronology and genesis of gold mineralization in Nurt of Northern Altay, Xinjiang: A case study on the Aketishikan gold deposit. Acta Geol Sin-Engl Ed, 2004, 78(2): 562−567

8 Qin K Z, Sun S, Li J L, et al. Eight stages of major ore deposits in northern Xinjiang, NW-China: Clues and constraints on the tectonic evolution and continental growth of Central Asia. In: Mao J, Bierlein F P, eds. Mineral Deposit Research: Meeting the Global Challenge. Berlin, Heidelberg, New York: Springer, 2005. 1327−1330

9 Xu J, Xie Y, Zhong C, et al. Fluid inclusions in gold mineralization

in the Sarekoubu area of the southern Altai Mountains, Xinjiang, China. In: Mao J, Bierlein F P, eds. Mineral Deposit Research: Meeting the Global Challenge. Berlin, Heidelberg, New York: Springer, 2005. 1359－1362

10 Zhang Z H, Mao J W, Du A D, et al. Magmatic Cu-Ni sulfide deposits in northern Xinjiang, China: A review. In: Mao J, Bierlein F P, eds. Mineral Deposit Research: Meeting the Global Challenge. Berlin, Heidelberg, New York: Springer, 2005. 1373－1375

11 Han C M, Xiao W J, Zhao G C, et al. Major types, characteristics and geodynamic mechanism of Upper Paleozoic copper deposits in northern Xinjiang, northwestern China. Ore Geol Rev, 2006, 28(3): 308－328[doi]

12 Mao J W, Pirajno F, Zhang Z H, et al. A review of the Cu-Ni sulphide deposits in the Chinese Tianshan and Altay orogens (Xinjiang Autonomous Region, NW China): Principal characteristics and ore-forming processes. J Asian Earth Sci, 2008, 32(2-4): 184－203

13 Pirajno F, Mao J W, Zhang Z C, et al. The association of mafic-ultramafic intrusions and A-type magmatism in the Tian Shan and Altay orogens, NW China: Implications for geodynamic evolution and potential for the discovery of new ore deposits. J Asian Earth Sci, 2008, 32(2-4): 165－183

14 Kovalenko V, Yarmolynk V, Bogatikov O. Magmatism, Geodynamics, and Metallogeny of Central Asia. Muscow: MIKO-Commercial Herald Publisher, 1995

15 Xiao W J, Windley B F, Yuan C, et al. Paleozoic multiple subduction-accretion processes of the southern Altaids. Am J Sci, 2009, 309: 221－270[doi]

16 Xiao W J, Windley B F, Badararch G, et al. Paleozoic accretionary and convergent tectonics of the southern Altaids: Implications for the growth of central Asia. J Geol Soc London, 2004, 161: 1－4[doi]

17 GCRSX (Group for Compilation of Regional Stratigraphy of Xinjiang) eds. Regional Stratigraphic Table of NW China: Xinjiang Uygur Autonomous Region Fascicule (in Chinese). Beijing: Geological Publishing House, 1981

18 Wang G Y. The discovery of Sinian strata in Xinjiang Altay and its significance (in Chinese). Reg Geol China, 1983, 10: 117－119

19 Peng C E. Discovery and geological significance of micropaleoflora fro the Habahe Group in Baikaba district of Xinjiang (in Chinese). Xinjiang Geol, 1989, 7: 19－22

20 BGMRX (Bureau of Geology and Mineral Resources of Xinjiang Uygur Autonomous Region), Regional Geology of Xinjiang Uygur Autonomous Region. People's Republic of China, Ministry of Geology and Mineral Resources (in Chinese). Geological Memoirs, Series 1, No. 32, Beijing: Geological Publishing House, 1993

21 Long X P, Sun M, Yuan C, et al. U-Pb and Hf isotopic study of zircons from metasedimentary rocks in the Chinese Altai: Implications for Early Paleozoic tectonic evolution. Tectonics, 2007, 26: TC5015[doi]

22 Long X P, Sun M, Yuan C, et al. Early Paleozoic sedimentary record of the Chinese Altai: Implications for its tectonic evolution. Sediment Geol, 2008, 208(3-4): 88－100[doi]

23 Yuan C, Sun M, Xiao W J, et al. Accretionary orogenesis of the Chinese Altai: Insights from Paleozoic granitoids. Chem Geol, 2007, 242: 22－39[doi]

24 Sun M, Yuan C, Xiao W J, et al. Zircon U-Pb and Hf isotopic study of gneissic rocks from the Chinese Altai: Progressive accretionary history in the early to middle Paleozoic. Chem Geol, 2008, 247: 352－383[doi]

25 Li H J, He G Q, Wu T R, et al. Confirmation of Altai-Mongolia microcontinent and its implications (in Chinese). Acta Petrol Sin, 2006, 22: 1369－1379

26 Li T D, Poliyangsiji B H. Tectonics and crustal evolution of Altai in China and Kazakhstan (in Chinese). Xinjiang Geol, 2001, 19: 27－32

27 Chen Y C, Ye Q T, Wang J B, et al. Geology of ore deposits, metallogenic regularity and technoenocomic evaluation on the Altay metallogenic belt, Xinjiang area, China (in Chinese). Beijing: Geological Publishing House, 2003

28 Wang Z G, Zhao Z H, Zou T R. Geochemistry of Granitoids of the Chinese Altai (in Chinese). Beijing: Science Press, 1988

29 Wang T, Jahn, B M, Kovach V P, et al. Nd-Sr isotopic mapping of the Chinese Altai and implications for continental growth in the Central Asian Orogenic Belt. Lithos, 2009[doi]

30 Wang T, Hong D W, Jahn B M, et al. Timing, petrogenesis, and setting of Paleozoic synorogenic intrusions from the Altai Mountains, Northwest China: Implications for the tectonic evolution of an accretionary orogen. J Geol, 2006, 114: 735－751[doi]

31 Cai K D. Time of magmatism, Petrogenesis and the Tectonic Implication of the Western Chinese Altai Orogen, Northwest China (in Chinese). Thesis for Masteral Degree. Beijing: Graduate University of the Chinese Academy of Sciences, 2007

32 Tong Y, Wang T, Kovach V P, et al. Age and origin of the Takwshiken postorogenic alkali-rich intrusive rocks in southern Altai, near the Mongolian border in China and its implications for continental growth (in Chinese). Acta Petrola Sin, 2006, 22(5): 1267－1278

33 Zhou G, Zhang Z C, Luo S B, et al. Confirmation of high-temperature strongly peraluminous Mayin'ebo granites in the south margin of Allay, Xinjiang: Age, geochemistry and tectonic implications (in Chinese). Acta Petrola Sin, 2007, 23(8): 1909－1920

34 Tong Y, Wang T, Hong D W, et al. Ages and origin of the early Devonian granites from the north part of Chinese Altai mountains and its tectonic implications (in Chinese). Acta Petrola Sin, 2007, 23(8): 1933－1944

35 Zhao Z H, Wang Q, Xiong X L, et al. Magnesian igneous rocks in northern Xinjiang (in Chinese). Acta Petrola Sin, 2007, 23(7): 1696－1707

36 Niu H C, Hiroaki S, Zhang H X, et al. Juxtaposition of adakite, boninite, high-TiO_2 and low-TiO_2 basalts in the Devonian southern Altay, Xinjiang, NW China. J Asian Earth Sci, 2006, 28: 439－456[doi]

37 Briggs S M, Yin A, Manning C E, et al. Late paleozoic tectonic history of the ertix fault in the chinese altai and its implications for the development of the central Asian orogenic system. Geol Soc Am Bull, 2007, 119(7-8): 944－960[doi]

38 Xu J F, Castillo P R, Chen F R, et al. Geochemistry of late Paleozoic mafic igneous rocks from the Kuerti area, Xinjiang, northwest China: Implications for backarc mantle evolution. Chem Geol, 2003, 193(1-2): 137－154

39 Zhang H X, Niu H C, Terada K, et al. Zircon SHRIMP U-Pb dating on plagiogranite from Kuerti ophiolite in Altay, North Xinjiang (in Chinese). Chin Sci Bull, 2003, 48(20): 2231－2235

40 Zhu Y F, Zeng Y S, Gu L B. Geochemistry of the rare metal-bearing pegmatite No. 3 vein and related granites in the Keketuohai region, Altay Mountains, northwest China. J Asian Earth Sci, 2006, 27: 61－77[doi]

41 Yuan C, Sun M, Long X P, et al. Constraining the deposition time and tectonic background of the Habahe Group of the Chinese Altai (in Chinese). Acta Petrol Sin, 2007, 23(7): 1635－1644

42 Brown M. Crustal melting and granite magmatism: Key issues. Phys Chem Earth, 1998, 26: 201－212[doi]

43 Sisson V B, Pavlis T L, Roeske S M, et al. Introduction: An overview of ridge-trench interaction in modern and ancient settings. In: Sisson V B, Roeske S M, Pavlis T L, eds. Geology of A Transpressional Orogen Developed during Ridge-trench Interaction along the North Pacific Margin. Geol Soc Am Spec Paper, 2003, 371: 1－18

44 Windley B F, Alexeiev D, Xiao W J, et al. Tectonic models for accretion of the Central Asian Orogenic Belt. J Geol Soc London, 2007, 164: 31－47[doi]

45 Bouygois J, Martin H, Lagabrielle Y, et al. Subduction erosion related to spreading-ridge subduction: Taitao peninsula (Chile margin triple junction area). Geology, 1996, 24: 723－726[doi]

46 Sample J C, Reid M R. Large-scale, latest Cretaceous uplift along the northeast Pacific Rim: Evidence from sediment volume, sandstone petrography, and Nd isotope signatures of the Kodiak Formation, Kodiak Island, Alaska. In: Sisson, V B, Roeske S M, Pavlis T L, eds. Geology of a Transpressional Orogen Developed during Ridge-trench Interaction along the North Pacific Margin. Geol Soc Am Spec Paper, 2003, 371(Special paper): 51－70

47 Trop J M, Ridgway K D, Spell T L. Sedimentary record of transpressional tectonics and ridge subduction in the Tertiary Matanuska Valley-Talkeetna Mountains forearc basin, southern Alaska. In: Sisson V B, Roeske S M, Pavlis T L, eds. Geology of a Transpressional Orogen Developed during Ridge-trench Interaction along the North Pacific Margin. Geol Soc Am Spec Paper, 2003, 371: 89－118

48 Browman J B, Sisson V B, Valley J W, et al. Oxygen isotope constraints on fluid infiltration associated with high-temperature-pressure metamorphism (Chugach metamorphic complex) within the Eocene southern Alaska forearc. In: Sisson, V B, Roeske S M, Pavlis T L, eds. Geology of a Transpressional Orogen Developed during Ridge-trench Interaction along the North Pacific Margin. Geol Soc Am Spec Paper, 2003, 371: 237－252

49 Zumsteg C L, Himmelbery G R, Karl S M, et al. Metamorphism within the Chugach accretionary complex on the southern Baranof Island, southeastern Alaska. In: Sisson V B, Roeske S M, Pavlis T L, eds. Geology of a Transpressional Orogen Developed during Ridge-trench Interaction along the North Pacific Margin. Geol Soc Am Spec Paper, 2003, 371: 253－268

50 Abratis M. Geochemical variations in magmatic rocks from the southern Costa Rica a consequence of Coco Ridge subduction and uplift of the Cordillera de Talamanca. Dissertation for Doctoral Degree. Gottingen: University of Gottingen, 1998

51 Thorkelson D J. Subduction of diverging plates and the principles of slab window formation. Tectonophysics, 1996, 255: 47－63[doi]

52 Stern C R, Kilian R. Role of the Subducted Slab, Mantle Wedge and Continental Crust in the Generation of Adakites from the Andean Austral Volcanic Zone. Contrib Mineral Petrol, 1996, 123: 263－281[doi]

53 Smithies R H. The Archaean tonalite-trondhjemite-granodiorite (TTG) series is not an analogue of Cenozoic adakite. Earth Planet Sci Lett, 2000, 182: 115－125[doi]

54 Prouteau G, Scaillet B, Pichavant M, et al. Evidence for mantle metasomatism by hydrous silicic melts derived from subducted oceanic crust. Nature, 2001, 410: 197－200[doi]

55 Wong P W, Sun M, Zhao G C, et al. Late Paleozoic ridge subduction along the southern margin of Chinese Altai and its implications on orogenesis and crustal growth. IGC, 2008

56 Wei C J, Clarke G, Tian W, et al. Transition of metamorphic series from the Kyanite- to andalusite-types in the Altai orogen, Xinjiang, China: Evidence from petrography and calculated KMnFMASH and KFMASH phase relations. Lithos, 2007, 96(34): 353－374

57 Niu H C, Yu Y X, Xu J F, et al. Late Paleozoic Volcanism and Associated Metallogenesis in the Altay area, Xinjiang, China (in Chinese). Beijing: Geological Publishing House, 2006